Geophysical Research Letter

Supporting Information for

The Complex Role of Storms in Modulating Intra-seasonal Air-Sea CO_2 Fluxes in the Sub-Antarctic Atlantic Southern Ocean.

Tesha Toolsee[1,2,*], Sarah-Anne Nicholson[1], Pedro M.S. Monteiro[3]

1 Southern Ocean Carbon-Climate Observatory (SOCCO), CSIR, Cape Town, South Africa

2 Department of Oceanography, University of Cape Town, Cape Town, South Africa

3 School for Climate Studies, Stellenbosch University, Stellenbosch, South Africa

*Corresponding author: Tesha Toolsee (TLSTES001@myuct.ac.za)

Contents of this file

1. Text S1 to S4
2. Figures S1 to S4

Introduction

This supplementary text (S1 to S4) provides additional and detailed information about the Southern Ocean Seasonal Cycle Experiment (SOSCEx) from which the glider data originate, and the data processing conducted on the glider data. Additionally, the methods used to calculate each parameter of the bulk CO_2 flux equation are explained in more detail in text S2. The supplementary figures (S1 to S4) show additional information referenced in the main text such as the different datasets used to identify the best fitted reanalysis wind product.

Text S1. Southern Ocean Seasonal Cycle Experiment (SOSCEx)

The Southern Ocean Seasonal Cycle Experiment (SOSCEx) initiated in 2012 is a multi-year observational programme designed to address the intra-seasonal to submesoscale uncertainty that connects the carbon cycle in the Southern Ocean to global climate variability (Swart et al., 2012). SOSCEx reflects a shift from historical ship-based observations to high-resolution autonomous sampling by gliders. These seasonal-long experiments involve simultaneous observations of the coupled air-sea and mixed-layer interface using twinned surface vehicles (Wave Gliders) and profiling buoyancy gliders (Seaglider).

Text S2. Estimation of the bulk CO_2 flux

k_w is governed by complex boundary layer processes that are largely controlled by wind speed (Ho et al. 2006, Wanninkhof, 2014). This relationship is based on the assumption that surface wind speed induces shear stress on the surface boundary layer of the ocean, triggering turbulence that has the ability to change the k_w. Consequently, k_w is commonly expressed as a function of wind speed (Wanninkhof, 1992, Sweeney et al., 2007, Blomquist et al., 2017). In the current study, due to the location of the Wave Gliders being in a high wind speed regime, a quadratic parameterization was used to estimate k_w (Ho et al. 2006, Wanninkhof, 2014).

$$\mathrm{K_w} = 0.251 < \mathrm{U^2} > \left(\frac{\mathrm{Sc}}{660}\right)^{-0.5} \quad (1)$$

where 0.251 cm hr^{-1} is the coefficient of gas transfer 'a', $<U^2>$ is the square of the wind speed (m s^{-1}) at 10 m from the ocean surface and Sc is the Schmidt number calculated using the methods described in Wanninkhof (2014). The impact of temperature dependence of the Schmidt number on the k_w throughout the Wave Gliders deployment showed to be minimal (r^2 = 0.006) and we could thus safely explain the majority of the intra-seasonal k_w variability from the wind speed (r^2 = 0.94).

The weather station on the Wave Glider, CSIR1, was however faulty and no usable atmospheric data is available from 14th August 2015 to 17th October 2015 in order to obtain $<U^2>$. Amongst four different reanalysis products; ECMWF Reanalysis v5 hourly reanalysis (ERA5; Hersbach et al. 2020), Japanese 55 years 3 hourly reanalysis (JRA-55; Tsujino et al. 2018), National Centres for Environment Predictions v2 6 hourly reanalysis (NCEP-II; Kanamitsu et al. 2002) and the Cross-Calibrated Multi-Platform v3 6 hourly reanalysis (CCMP; Mears et al. 2022), the hourly ERA5 was found to be the best-fitted product to replace the Wave Glider's atmospheric data ($r^2 = 0.788$; Figure S1b and c). Although Schmidt et al. (2017) found NCEP-II to be the best-performing reanalysis product for our study period and region, the newly available ERA5 hourly reanalysis product was not included in their analysis. Similarly, ERA5 wind stress data was used to highlight the passage of the storms in Figure 2.

k_o was calculated using an integrated van't Hoff formula expressed as follows (Weiss, 1974).

$$K_o = A_1 + A_2\left(\frac{100}{SST}\right) + A_3\left(\frac{SST}{100}\right) + S[B_2 + B_2\left(\frac{SST}{100}\right) + B_3\left(\frac{SST}{100}\right)^2] \quad (2)$$

Where A_1, A_2, A_3, B_1, B_2, and B_3 were obtained from Table 2 of Wanninkhof (2014).

The hourly xCO_{2air} and xCO_{2sea} measurements underwent quality control where outliers above the 99th percentile and lower 1st percentile of their discrete temporal difference were removed. pCO_{2air} (µatm) and $pCO_{2sea\_observed}$ (µatm) were both calculated using the following equation (Pierrot et al., 2009).

$$pCO_{2air/sea-observed} = xCO_{2air/sea}[P - pH_2O] \quad (3)$$

where P (atm) is the observed atmospheric pressure measured from the Wave Gliders, pH_2O (atm) is the water vapor pressure at the surface of the ocean and is calculated as follows (Weiss and Price, 1980).

$$pH_2O = e^{24.4543 - 67.4509\left(\frac{100}{T}\right) - 4.8489 \ln\left(\frac{T}{100}\right) - 0.000544S} \quad (4)$$

where T is the temperature inside the xCO_2 analyser (K), and S is the sea surface salinity (‰).

Although the xCO_2 analyser and the SST probe are located in close proximity to each other on the Wave Gliders, an empirical temperature correction was still conducted on $pCO_{2sea\_observed}$ to offset any disparity in the temperatures recorded inside the xCO_2 analyzer and the SST probe (Takahashi et al., 1993).

$$pCO_{2sea(temp\ corrected)} = pCO_{2sea-observed} e^{0.0423(SST-T)} \quad (5)$$

Finally, to obtain a thermodynamically correct and consistent pCO_{2sea}, the mean pCO_{2air} of the entire study period (392.524 µatm) was added to ΔpCO_2 ($pCO_{2sea(temp\ corrected)}$ - pCO_{2air}).

$$pCO_{2sea} = \Delta pCO_2 + 392.524\ \mu atm \quad (6)$$

Text S3. Calculation of Brunt-Väisälä Frequency (N^2) and Mixed Layer Depth (MLD)

N^2 (s^{-2}), also known as the buoyancy frequency, is the parameterization of stratification in the upper ocean (McDougall et al. 2003).

$$N^2 \equiv -\frac{g}{\rho}\frac{d\rho}{dz} \quad (9)$$

where ρ is the potential density, g is the gravitational acceleration and z is depth. Temperature and salinity data with depth from the Seaglider were used to calculate ρ.

MLD was defined as the depth where the density difference threshold first exceeds 0.03 kg m^{-3} from the surface (de Boyer Montégut et al. 2004; Dong et al. 2008). The MLD data was

smoothed with a 6-point rolling mean. The Python GliderTools package was used to calculate both N^2 and MLD (Gregor et al. 2019).

Text S4. Storm identification

The meteorological characteristics linked to the passage of storms are usually associated with a drop in the mean sea level pressure and a sudden change in the wind speed and direction. In the case of extratropical storms in the Southern Ocean, a set of meteorological criteria were defined to identify those storms (Figure S2). Periods of simultaneous wind speed exceeding 10 m s^{-1} (force 5 on the Beaufort scale) (Carranza et al. 2018) and a rate of change of atmospheric pressure (dP/dt) exceeding 0.1 hPa hr^{-1} (Wang et al., 2015; Bharti et al., 2019) were labelled as storms. These thresholds are useful for identifying the central part of the storm. However, to capture pre-storm and post-storm conditions the start and the end of each storm were identified as the wind stress minimum before and after the central part of the storm respectively. A total of 25 storm events were identified, out of which 6 occurred in winter, 7 in spring and 12 in summer.

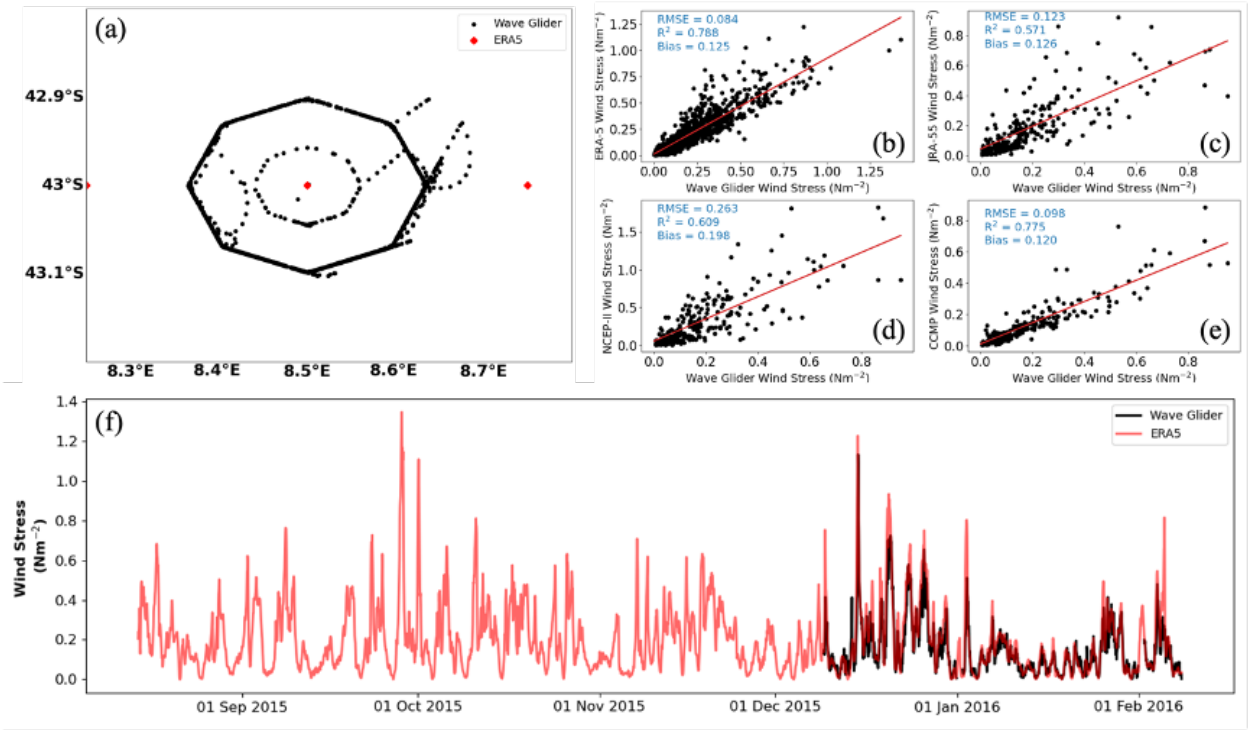

Figure S1. (a) Pseudo-mooring sampling pattern of the SOSCEX-III Wave Gliders (WG) centered around 8.5°E and 43°S in black and the spatial distribution of the gridded ERA5 reanalysis wind stress data in red. Linear regression analysis between (b) ERA-5 and WG, (c) JRA-55 and WG, (d) NCEP-II and WG, and (e) CCMP and WG. (f) Time series of ERA-5 wind stress (in red) and WG wind stress (in black) for their respective available duration.

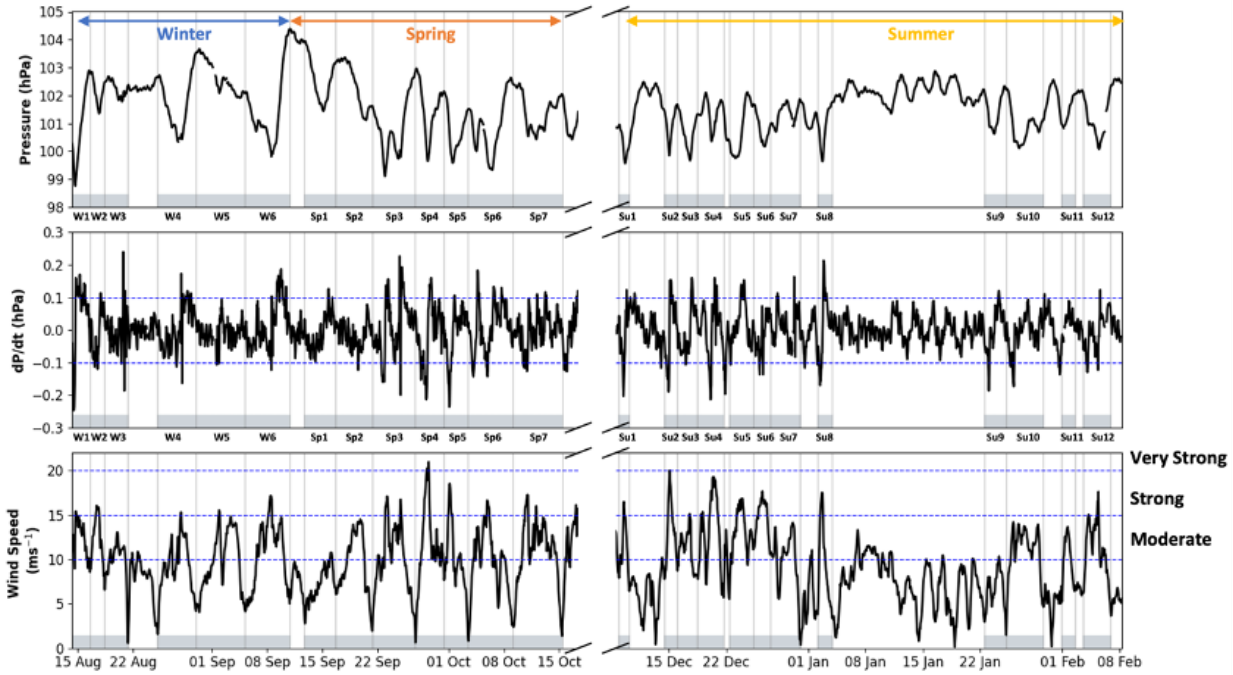

Figure S2. (a) Time series of (a) atmospheric pressure (hPa) recorded by the WG (b) Rate of change of Pressure (dP/dt; hPa), (c) ERA-5 wind speed (m s^{-1}) from 14th August 2015 to 17th October 2015 and 9th December 2015 to 8th February 2016. The grey shading represents the storm occurrences, and the gray lines separate each storm from one another.

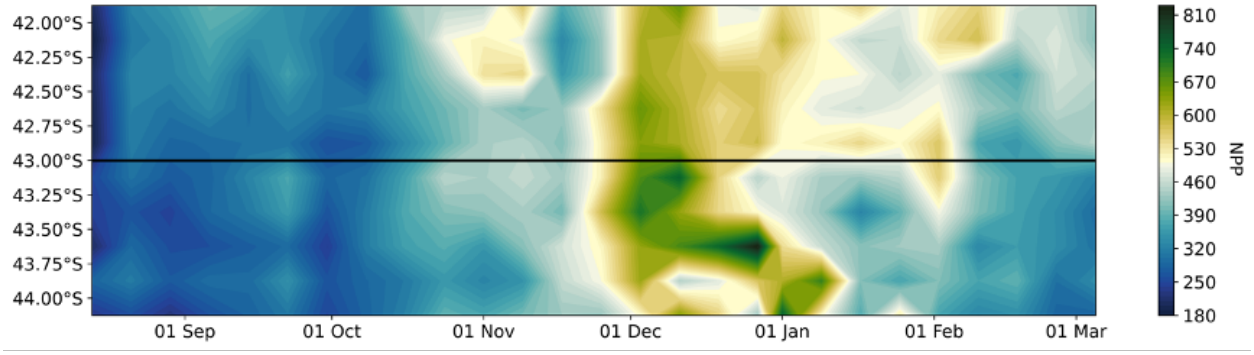

Figure S3: Hovmöller diagram of the Net Primary Productivity (NPP; mg C m^{-2} d^{-1}) estimated using the Carbon, Absorption, and Fluorescence Euphotic-resolving (CAFE) model from the version 6 of the Ocean Colour Climate Change Initiative (OCCCI v6). The solid black line refers to the location of the gliders' deployment. Note the low NPP (< 400 mg C m^{-2} d^{-1}) during late winter and spring and the high NPP (> 600 mg C m^{-2} d^{-1}) during summer at the gliders' location.

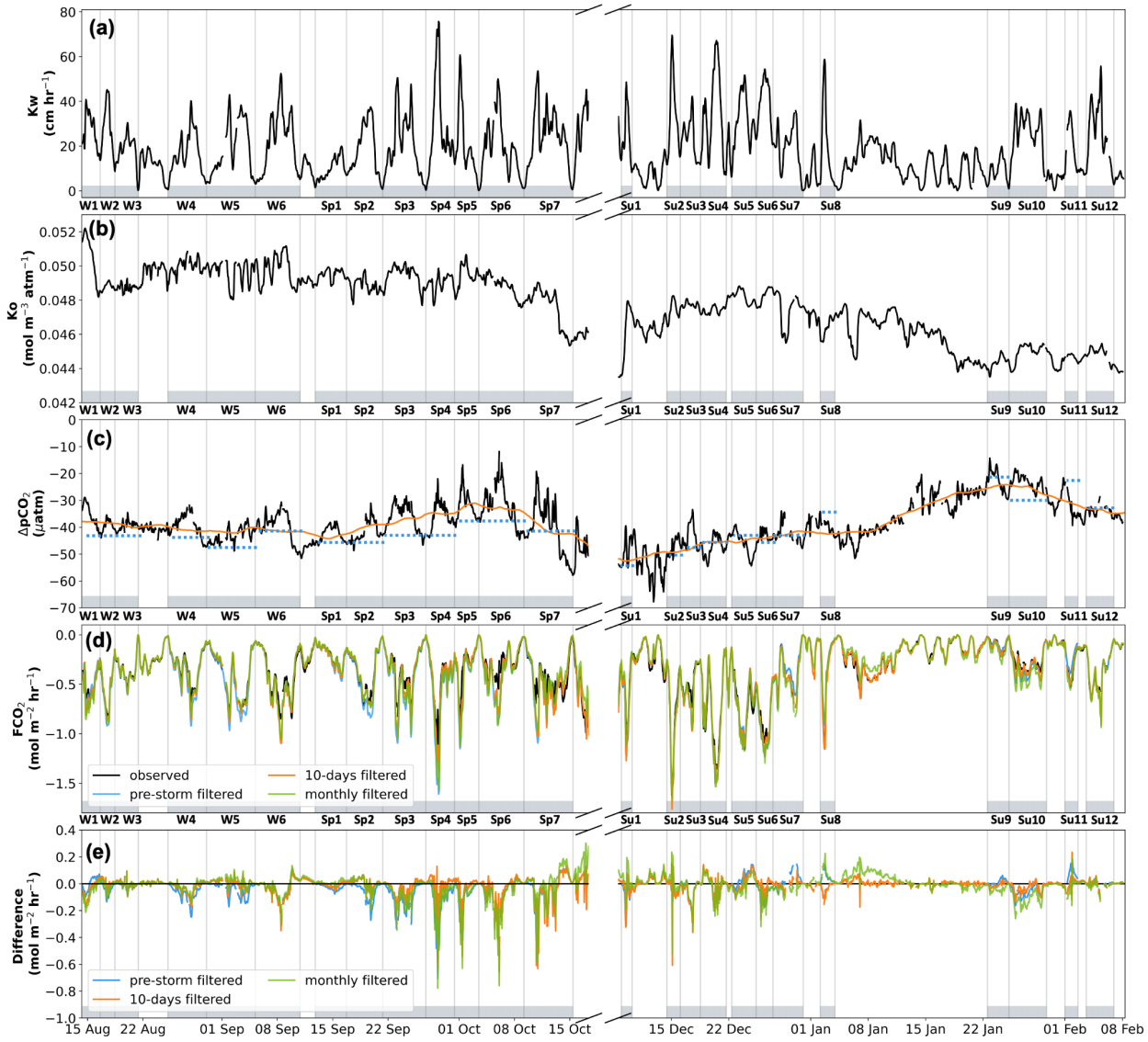

Figure S4: Time series of the **(a)** gas transfer coefficient, k_w (cm hr^{-1}), **(b)** solubility coefficient, k_o (mol L^{-1} atm^{-1}), **(c)** gradient in the partial pressure of CO_2 in the ocean and the atmosphere (ΔpCO_2 (μatm) = pCO_{2sea} (μatm) – pCO_{2air} (μatm)), with hourly ΔpCO_2 represented in black, 10-days rolling mean in ΔpCO_2 in orange and pre-storm values of ΔpCO_2 in blue, **(d)** CO_2 flux, FCO_2 (mol m^{-2} hr^{-1}) as observed by the Wave Gliders in black and the multiple filtered FCO_2 estimated using different sub-sampled ΔpCO_2, **(e)** difference between the observed FCO_2 and the filtered FCO_2 from the different methods used (mol m^{-2} hr^{-1}). All three experiments showed an overestimation of the FCO_2 but at slightly different magnitudes. The grey shading represents the storm occurrences, and the grey lines separate each storm from one another.

References

Bharti, V., Fairall, C.W., Blomquist, B.W., Huang, Y., Protat, A., Sullivan, P.P., Siems, S.T. and Manton, M.J. (2019). Air-sea heat and momentum fluxes in the Southern Ocean. Journal of Geophysical Research: Atmospheres, 124(23), 12426–12443, https://doi.org/10.1029/2018JD029761.

Blomquist, B.W., Brumer, S.E., Fairall, C.W., Huebert, B.J., Zappa, C.J., Brooks, I.M., Yang, M., Bariteau, L., Prytherch, J., Hare, J.E. and Czerski, H. (2017). Wind speed and sea state dependencies of air-sea gas transfer: Results from the High Wind speed Gas exchange Study (HiWinGS). Journal of Geophysical Research: Oceans, 122(10), 8034-8062, https://doi.org/10.1002/2017JC013181.

Carranza, M. M., Gille, S. T., Franks, P. J., Johnson, K. S., Pinkel, R., & Girton, J. B. (2018). When mixed layers are not mixed. storm-driven mixing and bio-optical vertical gradients in mixed layers of the Southern Ocean. Journal of Geophysical Research: Oceans, 123(10), 7264–7289, https://doi.org/10.1029/2018JC014416.

de Boyer Montégut, C., Madec, G., Fischer, A.S., Lazar, A. and Iudicone, D. (2004). Mixed layer depth over the global ocean: An examination of profile data and a profile-based climatology. Journal of Geophysical Research: Oceans, 109(C12), https://doi.org/10.1029/2004JC002378.

Dong, S., Sprintall, J., Gille, S.T. and Talley, L. (2008). Southern Ocean mixed-layer depth from Argo float profiles. Journal of Geophysical Research: Oceans, 113(C6), https://doi.org/10.1029/2006JC004051.

Gloege, L., McKinley, G.A., Landschützer, P., Fay, A.R., Frölicher, T.L., Fyfe, J.C., Ilyina, T., Jones, S., Lovenduski, N.S., Rodgers, K.B. and Schlunegger, S. (2021). Quantifying errors in observationally based estimates of ocean carbon sink variability. Global Biogeochemical Cycles, 35(4), p.e2020GB006788, https://doi.org/10.1029/2020GB006788.

Gregor, L., Lebehot, A.D., Kok, S. and Scheel Monteiro, P.M. (2019). A comparative assessment of the uncertainties of global surface ocean CO_2 estimates using a machine-learning ensemble (CSIR-ML6 version 2019a)–have we hit the wall?. Geoscientific Model Development, 12(12), 5113-5136, https://doi.org/10.5194/gmd-12-5113-2019.

Gregor, L., Ryan-Keogh, T.J., Nicholson, S.A., Du Plessis, M., Giddy, I. and Swart, S. (2019). GliderTools: A Python toolbox for processing underwater glider data. Frontiers in Marine Science, 6, 738, https://doi.org/10.3389/fmars.2019.00738.

Hersbach, H., Bell, B., Berrisford, P., Hirahara, S., Horányi, A., Muñoz-Sabater, J., Nicolas, J., Peubey, C., Radu, R., Schepers, D. and Simmons, A. (2020). The ERA5 global reanalysis. Quarterly Journal of the Royal Meteorological Society, 146(730), 1999-2049, https://doi.org/10.1002/qj.3803.

Ho, D. T., Law, C. S., Smith, M. J., Schlosser, P., Harvey, M., & Hill, P. (2006). Measurements of air-sea gas exchange at high wind speeds in the Southern Ocean: Implications for global parameterizations. Geophysical Research Letters, 33(16), https://doi.org/10.1029/2006GL026817.

Kanamitsu, M., Ebisuzaki, W., Woollen, J., Yang, S.K., Hnilo, J.J., Fiorino, M. and Potter, G.L. (2002). NCEP–DOE AMIP-II reanalysis (r-2). Bulletin of the American Meteorological Society, 83(11), 1631-1644, https://doi.org/10.1175/BAMS-83-11-1631.

McDougall, T.J., Jackett, D.R., Wright, D.G. and Feistel, R. (2003). Accurate and computationally efficient algorithms for potential temperature and density of seawater. Journal of Atmospheric and Oceanic Technology, 20(5), 730-741, https://doi.org/10.1175/1520-0426(2003)20<730:AACEAF>2.0.CO;2.

Mears, C., Lee, T., Ricciardulli, L., Wang, X. and Wentz, F. (2022). Improving the accuracy of the Cross-Calibrated Multi-Platform (CCMP) ocean vector winds. Remote Sensing, 14(17), 4230, https://doi.org/10.3390/rs14174230.

Pierrot, D., Neill, C., Sullivan, K., Castle, R., Wanninkhof, R., Lüger, H., Johannessen, T., Olsen, A., Feely, R.A. and Cosca, C.E. (2009). Recommendations for autonomous underway pCO_2 measuring systems and data-reduction routines. Deep Sea Research Part II: Topical Studies in Oceanography, 56(8-10), 512-522, https://doi.org/10.1016/j.dsr2.2008.12.005.

Schmidt, K.M., Swart, S., Reason, C. and Nicholson, S.A. (2017). Evaluation of satellite and reanalysis wind products with in-situ wave glider wind observations in the Southern Ocean. Journal of atmospheric and oceanic technology, 34(12), 2551-2568, https://doi.org/10.1175/JTECH-D-17-0079.1.

Sokolov, S. and Rintoul, S.R. (2009). Circumpolar structure and distribution of the Antarctic Circumpolar Current fronts: 1. Mean circumpolar paths. Journal of Geophysical Research: Oceans, 114(C11), https://doi.org/10.1029/2008JC005108.

Swart, S., Chang, N., Fauchereau, N., Joubert, W., Lucas, M., Mtshali, T., Roychoudhury, A., Tagliabue, A., Thomalla, S., Waldron, H. and Monteiro, P. (2012). Southern Ocean Seasonal Cycle Experiment 2012: Seasonal scale climate and carbon cycle links. South African Journal of Science, 108(3-4), 11-13, http://dx.doi.org/10.4102/sajs.v108i3/4.1089

Sweeney, C., Gloor, E., Jacobson, A.R., Key, R.M., McKinley, G., Sarmiento, J.L. and Wanninkhof, R. (2007). Constraining global air-sea gas exchange for CO_2 with recent bomb ^{14}C measurements. Global biogeochemical cycles, 21(2), https://doi.org/10.1029/2006GB002784.

Takahashi, T., Olafsson, J., Goddard, J. G., Chipman, D. W., & Sutherland, S. (1993). Seasonal variation of CO_2 and nutrients in the high-latitude surface oceans: A comparative study. Global Biogeochemical Cycles, 7(4), 843–878, https://doi.org/10.1029/93GB02263.

Takahashi, T., Sutherland, S.C., Sweeney, C., Poisson, A., Metzl, N., Tilbrook, B., Bates, N., Wanninkhof, R., Feely, R.A., Sabine, C. and Olafsson, J. (2002). Global sea–air CO_2 flux based on climatological surface ocean pCO_2, and seasonal biological and temperature effects. Deep Sea Research Part II: Topical Studies in Oceanography, 49(9-10), 1601–1622, https://doi.org/10.1016/S0967-0645(02)00003-6.

Thomalla, S.J., Fauchereau, N., Swart, S. and Monteiro, P.M.S. (2011). Regional scale characteristics of the seasonal cycle of chlorophyll in the Southern Ocean. Biogeosciences, 8(10), 2849-2866, https://doi.org/10.5194/bg-8-2849-2011.

Tsujino, H., Urakawa, S., Nakano, H., Small, R.J., Kim, W.M., Yeager, S.G., Danabasoglu, G., Suzuki, T., Bamber, J.L., Bentsen, M. and Böning, C.W. (2018). JRA-55 based surface dataset for driving ocean–sea-ice models (JRA55-do). Ocean Modelling, 130, 79-139, https://doi.org/10.1016/j.ocemod.2018.07.002.

Wang, Z., Siems, S. T., Belusic, D., Manton, M. J., & Huang, Y. (2015). A climatology of the precipitation over the Southern Ocean as observed at Macquarie Island. Journal of Applied Meteorology and Climatology, 54(12), 2321–2337, https://doi.org/10.1175/JAMC-D-14-0211.1.

Wanninkhof, R. (1992). Relationship between wind speed and gas exchange over the ocean. Journal of Geophysical Research: Oceans, 97(C5), 7373–7382, https://doi.org/10.1029/92JC00188.

Wanninkhof, R. (2014). Relationship between wind speed and gas exchange over the ocean revisited. Limnology and Oceanography: Methods, 12(6), 351–362, https://doi.org/10.4319/lom.2014.12.351.

Weiss, R. (1974). Carbon dioxide in water and seawater: the solubility of a non-ideal gas. Marine Chemistry, 2(3), 203–215, https://doi.org/10.1016/0304-4203(74)90015-2.

Weiss, R., & Price, B. (1980). Nitrous oxide solubility in water and seawater. Marine Chemistry, 8(4), 347–359, https://doi.org/10.1016/0304-4203(80)90024-9.